IEEE Access
Multidisciplinary | Rapid Review | Open Access Journal

Received February 14, 2019, accepted March 5, 2019, date of publication March 15, 2019, date of current version November 19, 2019.

Digital Object Identifier 10.1109/ACCESS.2019.2905345

2D-3D Registration With Weighted Local Mutual Information in Vascular Interventions

CAI MENG[1,2], QI WANG[1], SHAOYA GUAN[3], KAI SUN[1], AND BO LIU[1,2]

[1]School of Astronautics, Beihang University, Beijing 100191, China
[2]Beijing Advanced Innovation Center for Biomedical Engineering, Beihang University, Beijing 100191, China
[3]School of Mechanical Engineering and Automation, Beihang University, Beijing 100191, China

Corresponding author: Bo Liu (bo.liu@buaa.edu.cn)

This work was supported in part by the Key Projects of the NSFC under Grant 61533016 and Grant 61873010, and in part by the Young Scientists Project of NSFC under Grant 61601012.

ABSTRACT Registration between the intraoperative 2D digital subtraction angiography (DSA) and the preoperative 3D computed tomography angiography (CTA) is useful in the guidance of vascular interventional surgery (VIS). Because of the flow and diffusion of contrast in vessels, not all the vessels are visible in the DSA, which leads to difficulty in registration. Although the conventional mutual information (MI) and the normalized MI (NMI) perform well in orthopedic surgery, it cannot perform as well in VIS because of the missing vessel in DSA. In this paper, a novel similarity measure, WLMI (Weighted Local Mutual Information), is proposed to perform 2D-3D registration, which uses the patches selected in DSA to find the best match in the DRRs (digital radiography reconstruction) with weighted MI. At first, we choose several ways to measure the richness of block information to select small and scattered patches in the DSA image. Subsequently, different weights are assigned to these patches according to their information abundance by calculating the local MI. With the proposed WLMI, the 2D-3D registration experiments are conducted with the synthetic and real DSA images to CTA vessel model. In synthetic registration, the optimal way to measure information abundance and the optimal weight parameter value are selected. The registration with intact and partially absent vessels are compared with the conventional methods using MAE, mTREproj, and IoU metrics. In the registration of real DSA to CTA model, only IoU is used to compare the difference since the ground-truth cannot be derived. In synthetic registration with vessel excalation test, the mTREproj is 2.9 mm and the IoU is 96.7%. In a real registration test, the IoU reaches 81.3%. Both the synthetic and real DSA registration results show that the proposed WLMI can cope with the problem that partial vessel is invisible in the DSA, and outperformed the conventional methods such as MI and NMI. Therefore, the WLMI is more suitable to be used in the 2D/3D registration task in VIS.

INDEX TERMS 2D-3D registration, mutual information, weighted joint histogram, patch extraction.

I. INTRODUCTION

DSA (Digital Subtraction Angiography) is widely used in vascular interventional surgery (VIS). However, in DSA image the vessels are overlapped due to the central projection which further complicates the interventional procedure [1]. 3D vascular structure can be pre-extracted from CTA (Computed Tomography Angiography). Therefore, it is expected to align the DSA and CTA data to guide the VIS [1]–[4].

The key of registering 3D vascular model to 2D DSA is to derive their space transformation between CT and C-arm reference frame. C-arm can be regarded as pin-hole camera whose intrinsic parameters can be obtained from vendors, or by camera calibration. Therefore, the essence of registration is to calibrate the position and orientation of C-arm in reference to 3D model [6]. It is equivalent to solve a Perspective-n-Points problem [7], [8] where the point pairs are feature points on the 3D model and the DSA image. The features can be external artificial marker points or anatomical feature points such as bifurcation points of vascular centerline [5]. However, the field of view of C-arm is narrow which confines the placement of the markers. Furthermore, it is difficult to extract enough precise feature points because CTA and DSA/X-ray images have different dimensions and different image characteristics [9].

The associate editor coordinating the review of this manuscript and approving it for publication was Rajeswari Sundararajan.

Another approach of registering 3D vascular model to 2D DSA image is to convert the 2D-3D registration problem into 3D-3D registration [10], [11], or into 2D-2D registration [12]. As to the previous way, C-arm is rotated to acquire multi-angle DSA images to reconstruct the local 3D vessel model, and then the local model is registered to the global 3D vessel model reconstructed from CTA. However, the acquisition of multi-angle DSA increases the complexity of the surgery and operation time. As to the latter way, the 3D CTA vessel model is transformed into 2D DRRs (Digital Radiography Reconstruction) image under a series of pose transformation parameters. Then these DRRs are compared with the DSA image to find the best transformation that leads to the best similarity. It does not require extra apparatus operation, therefore it attracts more attention in research.

Mutual Information (MI) [17] is generally used to evaluate the similarity between the DRR and DSA. MI measures the strength of the statistical relationship between two images by using their joint probability distribution and is therefore robust to intensity discrepancy. MI performs well in 3D/2D registration in orthopedic surgery [13]. However MI only uses the gray intensity of each pixel and takes no consideration about other information. Therefore many other algorithms have been proposed to endow MI with spatial information, such as feature [23], local information [24], gradient [25], edge [26], orientation information [27]. Normalized Mutual Information (NMI) was introduced to handle the sensitivity overlap. The entropy calculation was also improved, including optimizing the calculation method of joint distribution [18], [19], estimating probability [20], adding weight to joint distribution. Cross-correlation [22] can also be combined with MI to improve the registration accuracy.

Although MI performs well in 2D/3D registration in orthopedic surgery, it doesn't perform as well as in VIS. At first, CTA can acquire clearer vasculature than DSA. There is no background noise in the DRRs from the CTA vessel 3D model compared with DSA; while in DSA, some organs or tissue may have similar intensity with vessel. Secondly, because of the incomplete flow and diffusion of contrast agent in vessels, some vessel branches that can be seen in 3D vessel model may be missing in DSA image. MI is calculated on the whole image, therefore it incorporates much undesired interference information. Furthermore, the vessel excalation (or partial missing vessel) may result in that the vessel information (edges and even orientations) extracted from DSA are inaccurate and hence not consistent with that in DRR. Subjected to these factors, the registration with MI is easy to fall into the wrong local extremum during optimization and fail to align the images [31].

Though some local MI metrics are proposed based on the gradient orientation [32] or distance to independent feature points [31], they do not take into account the effects of vessel excalation in the DSA and thus not suitable for 2D-3D registration in VIS. Therefore, in order to improve the accuracy of 2D-3D registration in VIS, a new similarity measure according to the characteristics of vascular images is expected to utilize local vascular information effectively and avoid the interference.

In this paper, a new similarity measurement, called weighted local mutual information (WLMI), is proposed based on MI. WLMI extracts local image blocks according to the defined information intensity and specific selection strategy, and calculates weighted normalized MI from these patches. By this method, most of the background-independent interference can be eliminated because the extracted image patches contain a lot of effective information. Besides, as the patches are extracted from the DSA and thus other possible features in the DRR are ignored, the effect of vessel excalation can also be avoided. What's more, the patch selection only relies on the information of the fixed image which needs just once calculation. Compared with the traditional MI metrics, WLMI can achieve better registration results.

We have introduced the idea in our previous conference paper [28]. In this paper, we discuss more about the patch selection and revise the weight calculation way. The framework of registration with WLMI is also updated. More experiments and analysis are supplemented to show the feasibility and robustness. The main contributions of the paper are:

(1) The local patches are selected according to the information abundance of the real DSA image, which helps eliminating the interference of other organs in the image background and the incoherence caused by vessel excalation in DSA image compared to DRR.

(2) An empirical weight equation is provided which is close to 1.0 but modified slightly. The modification is related to the information abundance of the selected patches.

(3) Based on the patch selection and weight computation, a new metric WLMI is proposed for the 2D-3D registration in VIS. It shows a better performance in evaluating the similarity between DSA and DRR in VIS registration.

The rest of this paper is organized as follows: Sec.2 introduces the 2D-3D registration framework and the methods used in this paper, including brief introduction of MI, feature patch extraction, local mutual information calculation. The registration experiment is conducted using the synthetic X-ray image and real image in Sec.3. For comparison, the results of conventional methods are also provided. The discussion and conclusion are followed in Sec.4 and Sec.5.

II. METHOD

2D-3D registration problem is usually transformed into 2D-2D registration. The framework of 2D-3D vascular registration can be divided into three steps: (1) Transform the preoperative 3D vascular model into a DRR image under given transformation parameters. (2) Compute the similarity between DRR and intraoperative DSA/X-ray image to judge whether the best similarity is achieved. If yes then registration succeeds, or else go to the next step. (3) Generate new transformation parameters with the appropriate search

optimization strategy and go to step (1) to iterate. If iteration exceeds maximum times, then registration fails.

A. 2D-3D REGISTRATION BASED ON SIMILARITY MEASURES

Denote $\boldsymbol{C}$ as the 3D vascular model obtained by CTA segmentation and reconstruction, I_{DSA} as the X-ray image to be registered. 2D-3D registration based on 2D-2D similarity measure is the process of finding the optimal transformation parameters $\boldsymbol{P}$ (including attitude angle R, position t, and intrinsic matrix K of C-arm camera) under which the transformed I_{DRR} from $\boldsymbol{C}$ by ray projection method [15] can have maximum similarity with I_{DSA}. The process can be expressed as

$$(\hat{R}, \hat{t}, \hat{K}) = \arg\max_{(R,t,K)} S\left(I_{DSA}, I_{DRR}\left(R, t, K, C\right)\right) \tag{1}$$

where $S(\cdot)$ represents similarity measure function to measure the quality of registration. $I_{DRR}\left(R, t, K, C\right)$ denotes the projective transformation of vascular model $\boldsymbol{C}$ under parameters R, t and K to obtain 2D image I_{DRR}, which can be expressed as

$$I_{DRR}(\boldsymbol{p}) = \int \mu(\boldsymbol{L}(\boldsymbol{p}, l) \cap C) dl \tag{2}$$

where $I_{DRR}(\boldsymbol{p})$ is the gray value of the DRR image at the point $\boldsymbol{p}$, $\boldsymbol{L}(\boldsymbol{p}, l)$ represents the ray from the virtual light source to the point $\boldsymbol{p}$ and their within distance l, $\mu(\cdot)$ is the X-ray attenuation coefficient.

Since the intrinsic matrix K of the C-arm used in clinic can be obtained by pre-calibration, Eq. 1 can be simplified to:

$$(\hat{R}, \hat{t}) = \arg\max_{(R,t)} S\left(I_{DSA}, I_{DRR}\left(R, t, C\right)\right) \tag{3}$$

B. SIMILARITY MEASURES

1) TRADITIONAL SIMILARITY MEASURES

In terms of Eq. 3, how to measure the similarity of I_{DSA} and I_{DRR} is the key. Traditional methods often use MI to measure similarity. Denote the intra-operative X-ray image I_{DSA} as the fixed image F, denote I_{DRR} as the floating image M, then their MI can be calculated by,

$$MI(F, M) = H(F) + H(M) - H(F, M) \tag{4}$$

where $H(X)$ is the marginal entropy of X that calculated according to the probability distribution $P(x)$ of gray intensity x; $H(F, M)$ is the joint entropy calculated according to the joint probability distribution of two images, defined as:

$$H(F, M) = \sum_{f,m} -P(f, m) \log P(f, m) \tag{5}$$

where (f, m) is the intensity pair of pixels occurs in corresponding pixel pairs and the joint probability distribution $P(f, m)$ can be estimated using joint histograms $h(f, m)$. The joint histogram $h(f, m)$ can be estimated by counting the number of times the intensity pair (f, m) occurs in the same position of two images, and then the joint distribution probability is estimated by the normalization of the histogram:

$$P(f, m) = \frac{h(f, m)}{\sum_{f,m} h(f, m)} \tag{6}$$

When the two images are correctly matched, MI reaches maximum. Since MI is sensitive to the size of overlapped parts, more robust NMI measure was introduced as:

$$NMI(F, M) = \frac{H(F) + H(M)}{H(F, M)} \tag{7}$$

2) WEIGHTED LOCAL MUTUAL INFORMATION (WLMI) MEASURE

For the vascular registration in VIS, due to the influence of complex background and vascular excalation, MI and NMI measure are easy to fall into the wrong local extremum in the process of optimization search which results in registration failure. Spatial information can be used to minimize the influence of background and vascular excalation. Based on this, the WLMI (weighted local mutual information) proposed in this paper is a combination of feature weight and local image mutual information.

In order to avoid the difference between the real DSA image and DRRs caused by vascular excalation and the complex background, one measure is to supplement the background of the DSA when generating DRR; the other is to use the information of the DSA to select the region with sufficient local information to participate in the registration and to ignore the regions with less information. The WLMI measure proposed in this paper adopts the latter way. Fixed image features are used to filter local image patches to obtain the mask image, then different weights of patches are added to estimate the joint distribution histogram. The NMI value calculated by DSA and DRR combining the mask image is used as the registration measure. In addition, the registration efficiency and accuracy can be further improved by giving different weights to different regions according to their information intensity.

a: SELECTION OF LOCAL PATCHES

In order to select patches with rich information, a feature value $V_{\boldsymbol{p}}$ should be defined for each pixel p to measure its information intensity or abundance in the fixed image F. With each pixel p as the center, r as the radius, a square window with $2r + 1$ side length is generated, and the region in the window is defined as a patch $\boldsymbol{L}_r(p)$. Assuming that D patches are selected for registration, and these patches are combined into a local region set $\boldsymbol{\Omega} = \{\boldsymbol{L}_r^i(p)\}, (i = 1, ..., D)$. However, due to the continuity of the image, if a point is rich in the information intensity, then its adjacent points are probably also rich. As a result, there is large overlap between adjacent patches, which results in relatively concentrated patches and less effective information. To make the selected patches distributed as much as possible, the overlap between adjacent patches should be restricted. Therefore, the patches can be

selected with such a strategy: (1) Sort the pixels of the image in descending order according to their V_p; (2) In the queued pixels, from begin to end, if pixel p's $\boldsymbol{L}_r(p)$ satisfies Eq.(8), then $\boldsymbol{L}_r(p)$ is added to $\boldsymbol{\Omega}$; (3) Repeat (2) until D patches are selected.

$$\boldsymbol{L}_r(p) \cap \boldsymbol{\Omega} < \eta \cdot Area\left(\boldsymbol{L}_r(p)\right) \tag{8}$$

where η is the allowable overlap rate of $\boldsymbol{L}_r(p)$ and the selected area. Large overlap rate will lead to excessive concentration of patches that cannot express the shape of vessels. In our method, η is set to 20% according to the experiment.

b: INFORMATION INTENSITY OF IMAGE PIXELS

In order to select patches, a feature value V_p should be defined to measure the richness of the information intensity for each pixel. The principle of patch selection is to preserve the useful information that has a great influence on the registration results, such as vessel edges, but avoid the parts that have less influence on registration result. There are three ways to measure the information abundance: (1) Gradient. The image gradient contains the shape information of the object, and larger gradients usually represent edges or corners; (2) Entropy. The entropy of the image characterizes the aggregation of the gray distribution of the image, and larger entropy can reflect more information; (3) Variance. The gray variance of the image represents the dispersion of the gray value, and larger variance usually represents higher contrast. Therefore, the information abundance in an image patch can be measured by the gradient (Eq.9), the entropy (Eq.10) or the gray variance (Eq.11):

$$g_{\boldsymbol{p}} = \sqrt{g_x^2 + g_y^2} \tag{9}$$

$$H_p = \sum_{(x,y)\in L_p} -P\left(I(x,y)\right) \log P\left(I(x,y)\right) \tag{10}$$

$$S_p = \frac{1}{N} \sum_{(x,y)\in L_p} \left(I_{(x,y)} - \overline{I}_{(x,y)}\right)^2 \tag{11}$$

where g_x, g_y is the sobel gradient of pixel I(x, y), $P\left(I(x, y)\right)$ is the probability of gray intensity $I(x, y)$, and $I(x, y)$ is the pixel value at the point (x, y) of the image. $\boldsymbol{L}_r(p)$ is the patch extracted from the fixed image, and N is the number of pixels in $\boldsymbol{L}_r(p)$.

c: WEIGHT CALCULATION

Local area $\boldsymbol{\Omega}$ based MI computation considers only pixels in D patches for both fixed and floating images in joint distribution histograms statistics. Joint distribution histograms usually are obtained by counting the number of occurrences of intensity pairs at the corresponding location in two images, which means that all pixels contribute equally to the histogram.

However, it is natural to think that the patch with rich information intensity should have more important role in similarity measurement. Therefore, it is necessary to give different weights to the patches involved in NMI calculation so as to make the regions with strong information intensity have higher weights. Weight $w_{\boldsymbol{p}}$ can be added to the $\boldsymbol{L}_r(p)$ to represent its importance in registration. Then the patch set can be represented as $\boldsymbol{\Gamma} = \{(w\left(p_i\right), \boldsymbol{L}_r(p_i)), i = 1, ..., D\}$. (The weight of all patches in $\boldsymbol{\Gamma}$ can be considered as $w\left(p\right) = 1$ when weight not considered, and it is defined as local mutual information LMI.) $w\left(p\right)$ is related to $V_{\boldsymbol{p}}$ and should not greatly affect the integrity of the joint distribution, thus Eq. (12) is used to calculate the weights. Pixels in each patch have the same weight $w\left(p\right)$. When calculating the joint distribution histogram, the number of pixels is replaced by the sum of the corresponding weights of pixels, as Eq.(13) shows. And then NMI is calculated as the final measure by Eqs. (5) and (7).

$$w\left(p\right) = 1 - \frac{1}{V_p^k} \tag{12}$$

$$P(f, m) = \frac{w\left(f\right) h\left(f, m\right)}{\sum\limits_{f,m} w\left(f\right) h\left(f, m\right)} \tag{13}$$

where k is the adjustment factor of joint histogram calculation weight.

The process of obtaining set $\boldsymbol{\Gamma}$ according to information abundance is equivalent to extracting features from fixed image $\boldsymbol{F}$. The proposed WLMI has following advantages: First, patch selection can avoid most of the irrelevant background organs and preserves the shape features of vessels. Second, the process of obtaining $\boldsymbol{\Gamma}$ only uses the information of fixed image $\boldsymbol{F}$, which reduces the computational complexity. Third, the proposed method can effectively avoid the influence of vessel excalation in DSA image, because only the features in the fixed image are extracted, and the positions of other possible features in the moving image are ignored.

C. 2D-3D REGISTRATION BASED ON WLMI

The 2D-3D registration process based on WLMI measure is shown in the Fig. 1.

At first, the region set $\boldsymbol{\Omega}$ and their weights $w_{\boldsymbol{p}}$ are calculated from the fixed image $\boldsymbol{F}$, which is recorded as a mask. Let I_{mask} be the mask image which has the same size as the fixed image $\boldsymbol{F}$. Initially I_{mask} are set to 0, indicating that no region is selected (or activated). The patch $\boldsymbol{L}_r(p)$ is then selected according to the patch selection strategy and the weights w_p is calculated. For each patch selected, all the pixels within the corresponding region in the I_{mask} are set to the w_p, i.e. $I_{\text{mask}}\left(L_r(p)\right) = w_p$. Then the nonzero pixel in the I_{mask} show the selected region $\boldsymbol{\Omega}$, and their value are their weights. If a pixel belongs to multiple regions, its weight is the average of different region weights.

Secondly, the preoperative 3D vascular model is used to generate a DRR image under a specific transform parameter T_k (an initial transform parameter $T_0 = (R_0, t_0)$ should be provided), and the WLMI between the DRR and the intraoperative X-ray image is calculated. Then a new transform parameterT_{k+1} is generated by Powell optimization

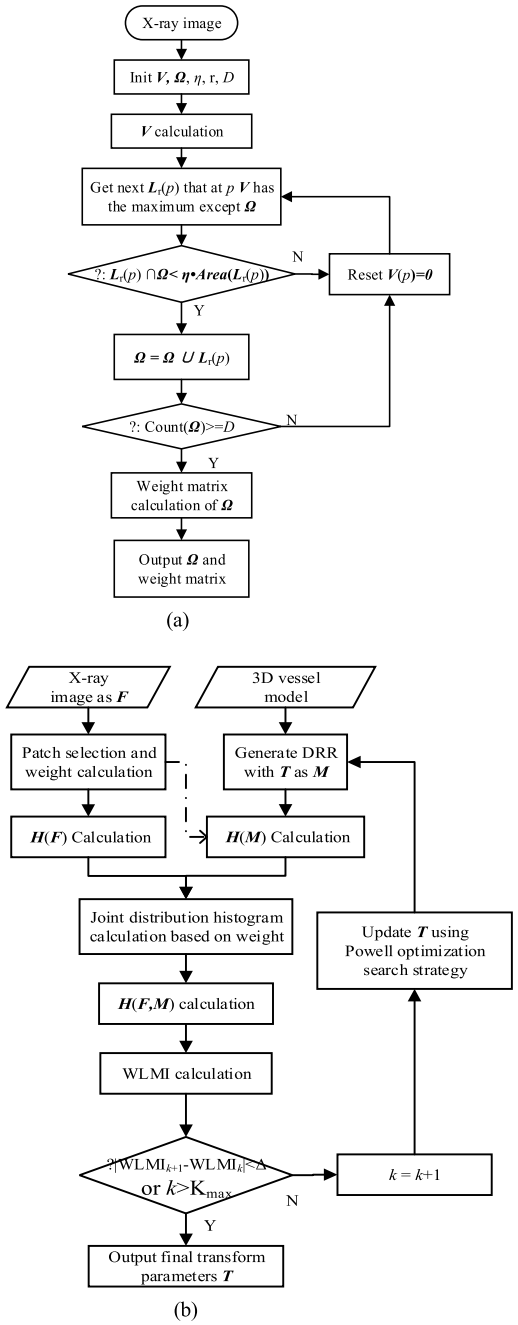

FIGURE 1. The registration framework with WLMI. (a) Patch selection and weight calculation. (b) Registration procedure.

search strategy. Iterate until the registration condition is satisfied, then the final registration parameters is obtained.

III. EXPERIMENTS AND RESULTS

In order to analyze and verify the proposed method, the registration experiments of 3D vascular model and simulated/real DSA images are conducted. At first, experiments are carried to select how to measure the information abundance in patch selection and the weight parameter k. Then registration experiments are conducted with synthetic and real DSA images respectively. In synthetic DSA image registration, intact and partial-missing vessels are used separately. The experimental

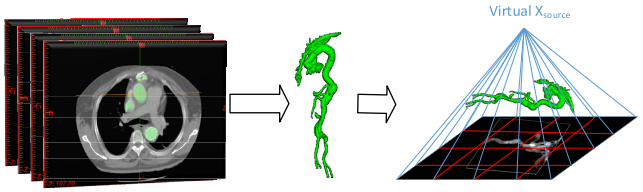

FIGURE 2. Reconstruction of 3D vascular model DRR generation.

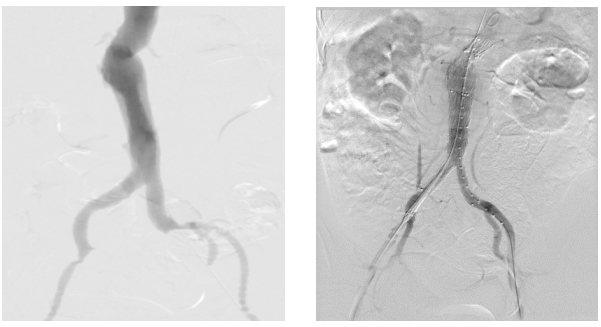

FIGURE 3. Synthetic DSA (a) and real DSA (b).

results show that the proposed WLMI achieves better registration results than other state-of-the-art metrics (MI, LMI and NMI).

A. DATA PREPARATION

The 3D vessel models are obtained from CTA images of two patients in Anzhen Hospital. The resolution of the CTA image is 194*122*611, and the physical size of the voxel is 0.68 *0.68*5 mm^3. Vascular segmentation is performed by threshold method, and the non-vascular part is erased manually by region growing algorithm. Finally, the 3D vascular model is reconstructed.

Fig. 2 shows procedure of reconstruction of the 3D vascular model from CTA imagery and generation of DRR. To quantify the registration accuracy, a simulated DSA image I^*_{DSA} is generated to work as fixed image $\boldsymbol{F}$. I^*_{DSA} is generated with the following equation:

$$I^*_{DSA} = \mu \cdot I_{bg} + \gamma \cdot G_\sigma * I_{DRR} + N(a, b) \qquad (14)$$

where I_{bg} is the background image generated from a real intraoperative DSA image sequence without injection of contrast medium. I_{DRR} is the DRR image generated by the vessel model under given transformation parameters which work as ground-truth, as shown in Fig.2. G_σ is a Gauss smoothing kernel with variance of σ, which is used to simulate the scattering effect of X-ray. $N(a, b)$ is uniformly distributed noise in interval $[a, b]$. μ and γ are the coefficients of synthesis. We adjust the parameters to make the synthetic images more similar to real DSA images. The simulation parameters used in the experiment are ($\mu = 0.6, \gamma = 0.8, \sigma = 0.5, a = -5, b = 5$). Fig. 3 (a) shows a synthetic X-ray image, whose resolution is 512*512 and pixel spacing is 0.74*0.74 mm^2.

Registration to the real DSA images of the patient are also conducted. The resolution of the DSA is 1024 * 1024, and the

pixel size is 0.37*0.37 mm^2. Fig. 3 (b) is the corresponding DSA image.

B. REGISTRATION RESULT EVALUATION

Ignoring the effect of vascular elastic deformation on registration accuracy, the main transform parameters considered in 3D space have six degrees of freedom, which can be expressed as $\mathbf{T} = (r_x, r_y, r_z, t_x, t_y, t_z)$, where (r_x, r_y, r_z) are the relative rotation angle around the X, Y, Z axis, and (t_x, t_y, t_z) are translation along X, Y, Z axis. Specially, t_z, the translation in Z axis is corresponding to the image zooming of the DRR.

DRRs are generated with random transform parameters shift whose rotation range is $\pm 10°$ and translation range is ± 10 mm with an initial reference position $\tilde{\mathbf{T}}$. Totally 10 synthetic DSA are generated for the simulated experiment.

Here the ground-truth registration parameters are $\tilde{\mathbf{T}}$, and the experiment result is $\mathbf{T}$. To evaluate the registration accuracy, the metrics of *mTREproj* (mean Target Registration Error in the projection direction), *MAE* (mean absolute error) and *IoU* (Intersection-over-Union) are adopted. *mTREproj* is the mean distance between reprojected points in the image, as shown in Eq.(15), where $P_n (n = 1, \ldots, N)$ are the N points selected in 3D vessel model, $\mathbf{T} \circ P_n$ and $\tilde{\mathbf{T}} \circ P_n$ mean re-project P_n into the image plane with registration parameters $\mathbf{T}$ and $\tilde{\mathbf{T}}$ respectively. *MAE* is shown as Eq.(16), where $\mathbf{T}_i(\tilde{\mathbf{T}}_i)$ is the i^{th} element in $\mathbf{T}(\tilde{\mathbf{T}})$. *IoU* is denoted in Eq.(17), where $area(I)$ represents the number of pixels constituting the vessels in the image I, I_1 and I_2 are the DRRs corresponding to $\mathbf{T}$ and $\tilde{\mathbf{T}}$ respectively. For the real image registration, because the ground-truth registration parameters cannot be obtained, only *IoU* will be used as the quantitative criterion. From the metrics, it can be seen that the less *mTREproj* is, or the less *MAE* is, or the higher the *IoU* is, the better the registration is achieved.

$$mTREproj = \frac{1}{N}\sum_{n=1}^{N}\left|\mathbf{T} \circ P_n - \tilde{\mathbf{T}} \circ P_n\right| \tag{15}$$

$$MAE_i = \frac{1}{N}\sum_{n=1}^{N}\left|\mathbf{T}_i - \tilde{\mathbf{T}}_i\right|, \quad i \in [1, 6] \tag{16}$$

$$IoU = \frac{area\,(I_1) \cap area\,(I_2)}{area\,(I_1) \cup area\,(I_2)} \tag{17}$$

C. INFORMATION MEASUREMENT AND WEIGHT SELECTION

1) INFORMATION MEASUREMENT

Three measurements of image information abundance (Eq. $(9 \sim 11)$) are tested to find the optimal way. In the comparison experiment, all the conditions are same only except the measurement. Fig.4 (a-f) shows one of the synthesized DSA images using different measurements to select the patches (empirical $D = 50$, $\eta = 20\%$, $r = 19$, $k = 1$).

Fig.5 shows the *MAE* of the six registration parameters under three measurements. It can be seen that all the three

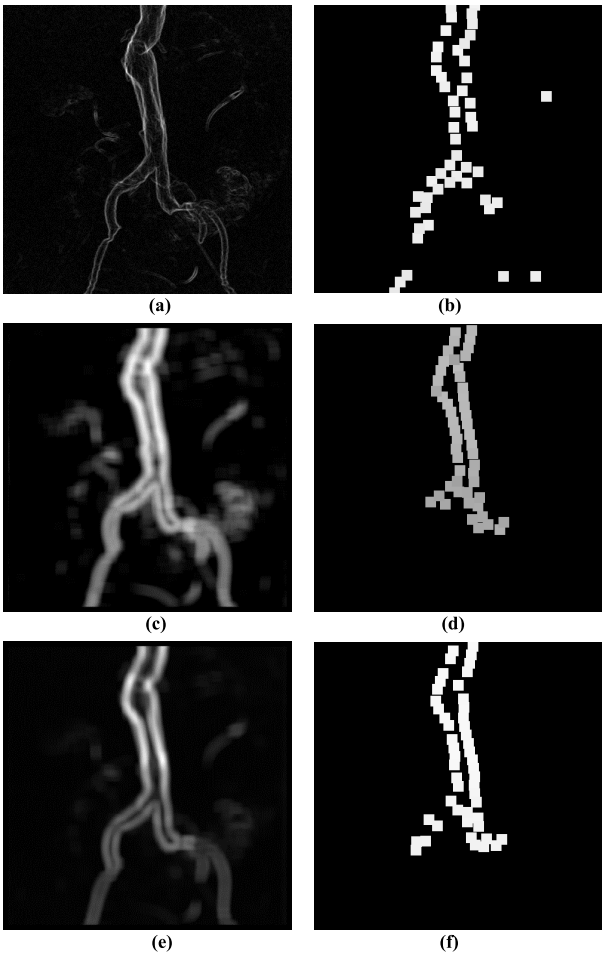

FIGURE 4. Information abundance maps and selected patches by different measurements. (a) Gradient map. (b) Selected patches by Gradient. (c) Entropy map. (d) Selected patches by Entropy. (e) Variance map. (f) Selected patches by Variance.

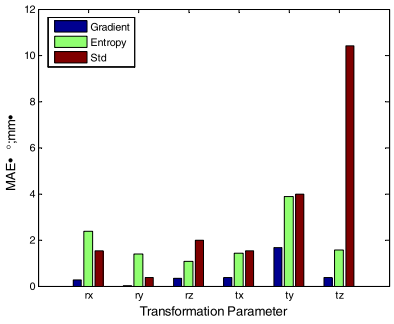

FIGURE 5. Comparison of registration results with different feature selection methods.

intensity measurements can work in 2D-3D registration. However, the *MAE* by Gradient is the smallest (position error is less than 2 mm, attitude error is less than 1 degree) compared with those by Entropy and Variance. The results show that the Gradient is the optimal measurement in registration.

2) WEIGHT PARAMETER k

The weight parameter k in Eq. (12) affects the weight computation. To find an optimal value, k is set to different values,

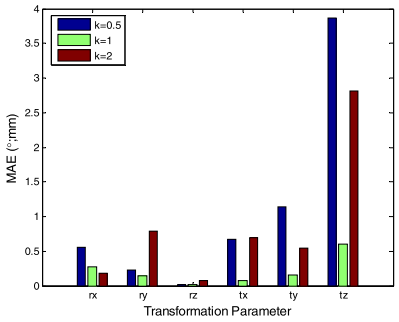

FIGURE 6. Comparison of registration results with different weighting *k*.

namely 0.5, 1, and 2. According to the above test, Gradient is chosen as the information measurement, and other parameters kept unchanged ($D = 50$, $\eta = 20\%$, $r = 19$). The *MAEs* of the registration results are shown in Fig.5.

From Fig.6 it can be drawn that all k work in the test. The bigger k is, the closer w_p is to 1. However, the *MAE* is not consistent with the change of k. Obviously $k = 1$ can retrieve better result than $k = 0.5$and $k = 2$, especially in t_z where the *MAE* of $k = 0.5$ or $k = 2$ is much larger than that of $k = 1$.

D. REGISTRATION EXPERIMENT OF SIMULATED DSA IMAGES

Because the registration parameters between real DSA images and 3D vessel model cannot be obtained, the registration experiments are carried out using the 10 simulated DSA images in order to quantitatively analyze the registration methods. In the registration experiment, the registration process based on WLMI is implemented by MATLAB, the DRR generation part is implemented by ITK. Ten groups of experiments are carried out. Moreover, the registration with conventional MI, WJH-MI, GMI, NMI and LMI are also implemented.

1) REGISTRATION EXPERIMENT WITHOUT VESSEL EXCALATION

First, a registration experiment with intact vessel was conducted. Fig.7 shows the overlay of the boundary of re-projection of 3D vessel model on the synthetic DSA image plane by the final Transform $\boldsymbol{T}$ and the DSA intrinsic parameters. Fig.8 shows the average statistical errors of the registration parameters. Table 1 shows the *mTREproj* and *IoU* result of these methods.

It can be seen that although all the methods can achieve the registration, the accuracy are different.

The maximum *MAE*, *mTREproj* and average iteration time of MI and NMI are all significantly higher than those of LMI and WLMI, indicating that the idea of local area registration has more advantages in vascular registration tasks. Besides, LMI, WLMI has better convergence effect on the parameter t_z representing the scaling effect, and the registration result is more stable.

2) REGISTRATION EXPERIMENT WITH VESSEL EXCALATION

In real DSA images, vessel may partly missing because of the diffusion effect of contrast. In order to simulate the vessel excalation, some ends of the 3D vascular model are wiped off intentionally and then the simulated DSA images are regenerated. The images are registered with the intact 3D vascular model. The other steps are same to the experiment without vessel excalation. Fig.9 shows the registration results. Fig.10 and Table 2 show the statistical results of the *MAE*, *mTREproj*, and *IoU*.

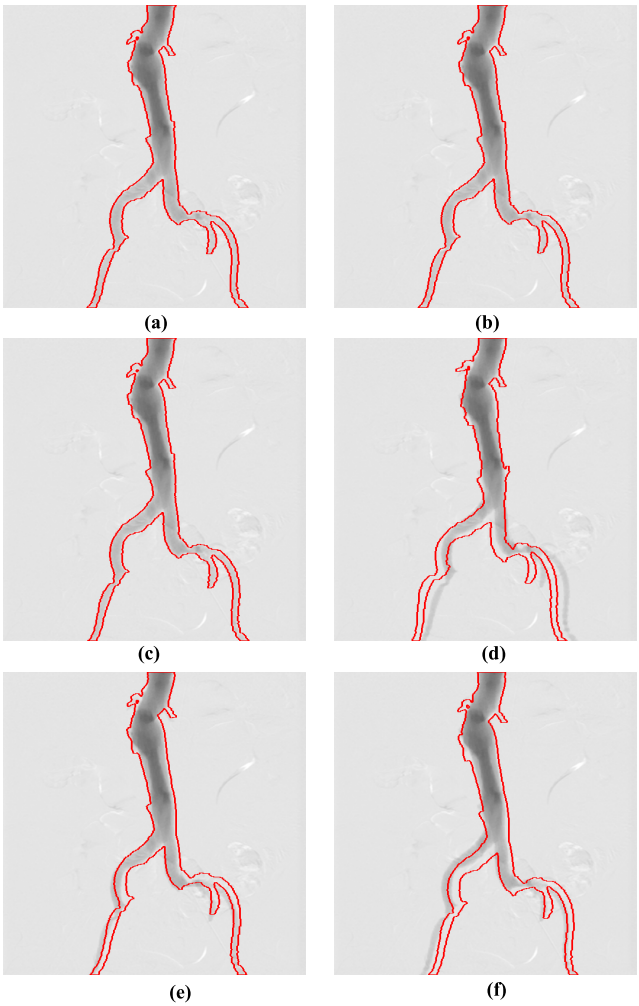

FIGURE 7. Registration results without vessel excalation by different metrics. The red contours in the image are the vascular boundaries in the DRR images corresponding to the registration result parameters. (a) WLMI. (b) LMI. (c) WJH-MI. (d) GMI. (e) NMI. (f) MI.

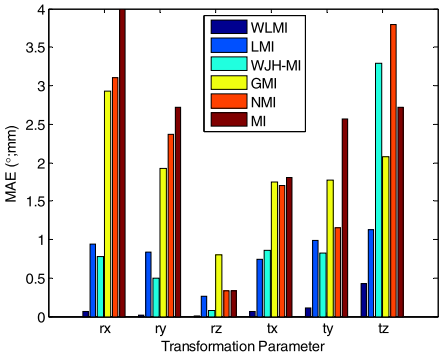

FIGURE 8. Comparison of MAE without vessel excalation.

TABLE 1. Registration comparison without vessel excalation.

	WLMI	LMI	MI_{WJH}	GMI	NMI	MI
mTREproj (mm)	**2.4**	6.4	7.6	8.7	22.7	24.7
IoU(%)	**99.5**	94.1	96.0	83.5	90.6	87.8

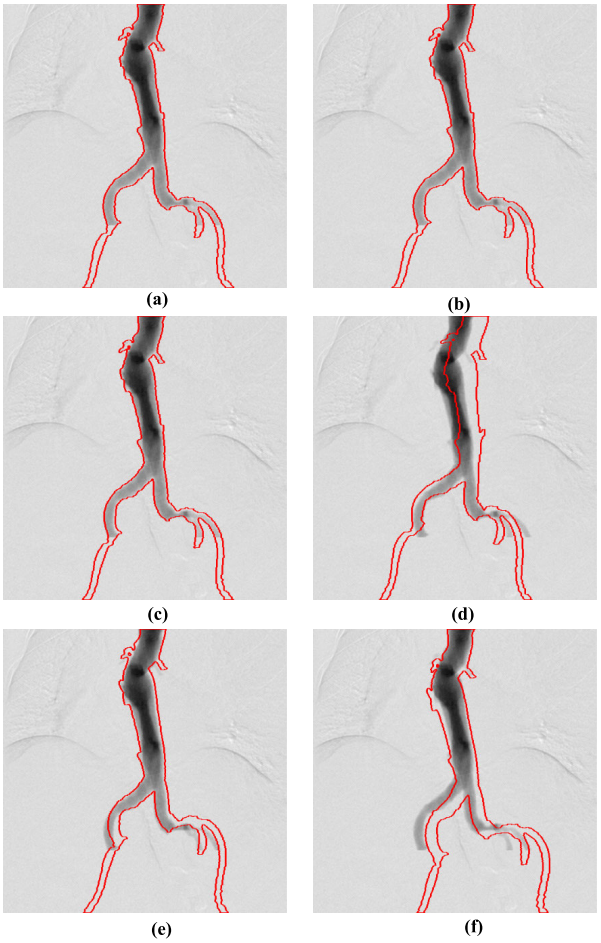

FIGURE 9. Registration results with vessel excalation by different metrics. The red contours in the image are the vascular boundaries in the DRR images corresponding to the registration result parameters. (a) WLMI. (b) LMI. (c) WJH-MI. (d) GMI. (e) NMI. (f) MI.

As can be seen from statistical results, the registration error has been increased because of vessel excalation. The maximum *MAE* of MI is greater than 10; therefore, it is regarded as failure. The *MAE* of NMI is larger than that of LMI and WLMI, and *mTREproj* of NMI is also one order of magnitude higher than that of LMI and WLMI. Experimental results show that WLMI and LMI based on feature patches are less susceptible to vascular excalation than NMI and MI, and can achieve registration more quickly and accurately. And registration based on WLMI is better than LMI.

3) NOISE ROBUSTNESS EXPERIMENT

In order to verify the robustness of WLMI registration method to noise, a group of noise experiments are carried out in this paper. According to Eq.(15), uniformly distributed noise is added to the fixed image I_F, and ten groups of experiments

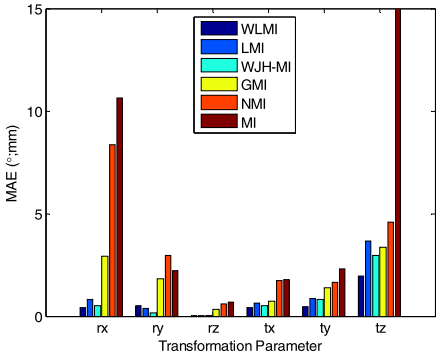

FIGURE 10. Comparison of MAE with vessel excalation.

TABLE 2. Registration comparison with vessel excalation.

	WLMI	LMI	MI_{WJH}	GMI	NMI	MI
mTREproj (mm)	**2.9**	6.4	9.3	16.2	37.1	-
IoU(%)	**96.7**	95.7	95.9	79.2	84.4	70.4

($a \in [0, 10]$) are carried out under the same conditions. The experimental results are shown in Fig.11.

$$I_{F-noise}(x, y) = \begin{cases} 255, & I_F(x, y) + rand(-a, a) > 255 \\ 0, & I_F(x, y) + rand(-a, a) < 0 \\ I_F(x, y) + rand(-a, a) & other \end{cases} \tag{18}$$

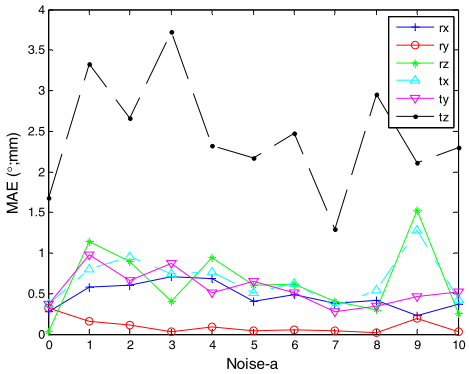

FIGURE 11. Registration error under different noise levels.

It can be seen from the Fig.11 that although the noise has a little impact on the registration results, the registration error is relatively stable.

From the synthetic registration experiment, it can be drawn that:

(1) If there is no vessel excalation, all measurements can be used in the VIS 2D-3D registration task. But the proposed metrics WLMI performs better than other MI-based metrics.

(2) Vessel excalation will lead to larger registration error compared with intact vessel. However, the proposed WLMI still surpasses other MI-based metrics.

(3) The noise in the image intensity has little effect on the proposed registration. The proposed WLMI is robust to image intensity noise.

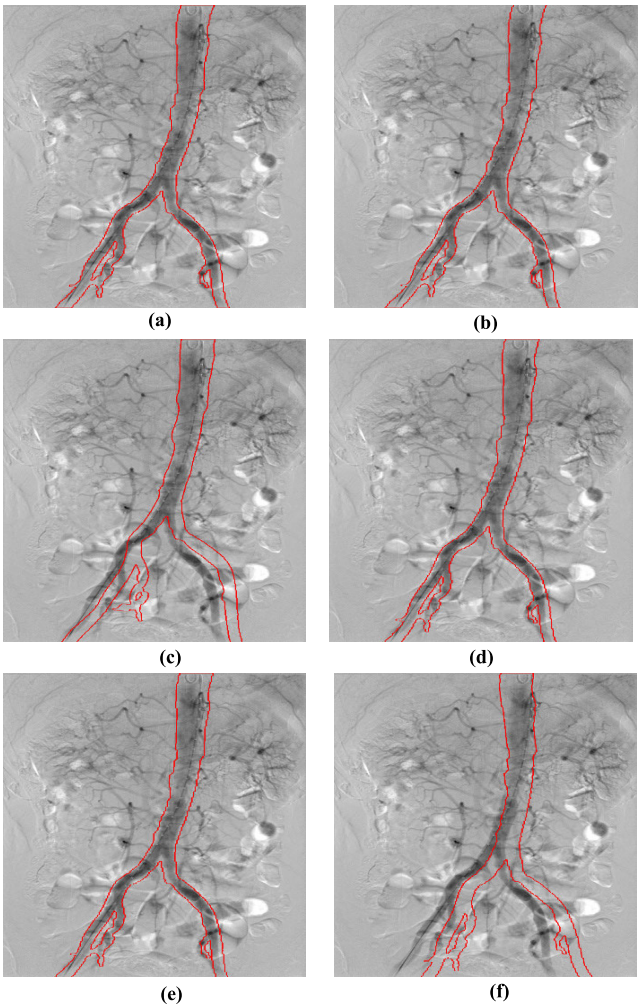

FIGURE 12. The registration result of WLMI for real vessel image. The red contour line is the edge of vessel in DRR corresponding to the registration result parameter, and the background is the real DSA image. (a) WLMI. (b) LMI. (c) WJH-MI. (d) GMI. (e) NMI. (f) MI.

TABLE 3. Registration comparison with real DSA image.

	WLMI	LMI	WJH-MI	GMI	NMI	MI
IoU (%)	**81.3**	80.8	58.1	77.5	77.6	47.1

E. REGISTRATION EXPERIMENTS OF REAL DSA IMAGES

In order to verify the registration effect in the actual situation, it is necessary to verify the feasibility and effectiveness of the proposed method in real surgical environment. Fig.12 shows the registration result of two patient. The background is the real DSA image and the red contour line is the registration result. Table 3 is the comparison of average *IoU*. The ground truth area of the real DSA are manually marked out. Figures show that the result of WLMI is basically consistent with the contours of vessels in real image, and the results of WLMI and LMI registration based on local information are obviously better than those of NMI and MI.

IV. DISCUSSION

Vessel excalation or the missing of some part of the vessels in DSA image, results in that there are significant information difference in DSA and DRR. Therefore global similarity measurement is slow in registration and easy to fall into wrong extremum. WLMI is more effective and faster than the traditional method in registration during VIS, because it just selects the patches with rich information that are highly probable existent both in DSA and DRR. Compared with the traditional MI or NMI, WLMI has greater gradient and is easier to converge under the same conditions. Furthermore, the selected patches can also reduce the influence of the background difference. The computational complexity of extracting the image patches can be reduced too. However, Besides similarity measure, the accuracy of segmentation, the clarity and contrast of vessels in DSA images will all affect the final registration results.

In the implementation, DRR image generation is realized by ITK program, and then is invoked in MATLAB according to the parameters given by Powell optimization. Most of registration time is consumed in the generation of DRRs. The functions in ITK can be accelerated by CUDA to shorten the generation time of DRR image, then the registration can be effectively accelerated.

V. CONCLUSION

This paper presents a new similarity measure WLMI to register preoperative 3D CT vessel model to intraoperative 2D X-ray images in VIS. WLMI incorporates MI algorithm and spatial information. Local patches are selected using the gradient of DSA image, which is in essence a particular sampling way to filter the information. Then the weights are assigned to each patch according to the gradient of the patch center. WLMI value is evaluated in these patches using weighted joint histogram. We test out results on both synthetic and real X-ray images, which show that the proposed WLMI measure is more accurate than traditional ways. In synthetic registration with vessel excalation test, the *mTREproj* is 2.9mm and the *IoU* is 96.7%. In real registration test, the *IoU* reaches 81.3%. Therefore, WLMI is more suitable to be used in 2D/3D registration task in VIS.

REFERENCES

[1] D. Rivest-Henault, H. Sundar, and M. Cheriet, "Nonrigid 2D/3D registration of coronary artery models with live fluoroscopy for guidance of cardiac interventions," *IEEE Trans. Med. Imag.*, vol. 31, no. 8, pp. 1557–1572, Aug. 2012.

[2] C. T. Metz *et al.*, "Registration of $3D + t$ coronary CTA and monoplane $2D + t$ X-ray angiography," *IEEE Trans. Med. Imag.*, vol. 32, no. 5, pp. 919–931, May 2013.

[3] J. Kim, J. Lee, J. W. Chung, and Y.-G. Shin, "Locally adaptive 2D–3D registration using vascular structure model for liver catheterization," *Comput. Biol. Med.*, vol. 70, pp. 119–130, Mar. 2016.

[4] Y. Khoo and A. Kapoor, "Non-iterative rigid 2D/3D point-set registration using semidefinite programming," *IEEE Trans. Image Process.*, vol. 25, no. 7, pp. 2956–2970, Jul. 2016.

[5] S.-Y. Guan, T.-M. Wang, C. Meng, and J.-C. Wang, "A review of point feature based medical image registration," *Chin. J. Mech. Eng.*, vol. 31, no. 1, p. 76, 2018.

[6] H. Shirato *et al.*, "Four-dimensional treatment planning and fluoroscopic real-time tumor tracking radiotherapy for moving tumor," *Int. J. Radiat. Oncol. Biol. Phys.*, vol. 48, no. 2, pp. 435–442, 2000.
[7] J. A. Hesch and S. I. Roumeliotis, "A direct least-squares (DLS) method for PnP," in *Proc. Int. Conf. Comput. Vis.*, Nov. 2011, pp. 383–390.
[8] S. Li, C. Xu, and M. Xie, "A robust O(n) solution to the perspective-n-point problem," *IEEE Trans. Pattern Anal. Mach. Intell.*, vol. 34, no. 7, pp. 1444–1450, Jul. 2012.
[9] T. S. Y. Tang, R. E. Ellis, and G. Fichtinger, "Fiducial registration from a single X-ray image: A new technique for fluoroscopic guidance and radiotherapy," in *Proc. Int. Conf. Med. Image Comput. Comput.-Assist. Intervent.* Berlin, Germany: Springer, 2000, pp. 502–511.
[10] J. Wang, A. Borsdorf, B. Heigl, T. Köhler, and J. Hornegger, "Gradient-based differential approach for 3-D motion compensation in interventional 2-D/3-D image fusion," in *Proc. 2nd Int. Conf. 3D Vis.*, Dec. 2014, pp. 293–300.
[11] A. Brost, R. Liao, J. Hornegger, and N. Strobel, "3D model-based catheter tracking for motion compensation in EP procedures," *Proc. SPIE*, vol. 7625, pp. 762507-1–762507-12, Feb. 2010.
[12] R. Schaffert, J. Wang, A. Borsdorf, J. Hornegger, and A. Maier, "Comparison of rigid gradient-based 2D/3D registration using projection and back-projection strategies," in *Bildverarbeitung für die Medizin*. Berlin, Germany: Springer, 2016.
[13] P. Markelj, D. Tomaževič, B. Likar, and F. Pernuš, "A review of 3D/2D registration methods for image-guided interventions," *Med. Image Anal.*, vol. 16, no. 3, pp. 642–661, 2012.
[14] L. Duong, R. Liao, H. Sundar, B. Tailhades, A. Meyer, and C. Xu, "Curve-based 2D-3D registration of coronary vessels for image guided procedure," *Proc. SPIE*, vol. 7261, Mar. 2009, Art. no. 72610S.
[15] S. Miao, Z. J. Wang, Y. Zheng, and R. Liao, "Real-time 2D/3D registration via CNN regression," in *Proc. IEEE 13th Int. Symp. Biomed. Imag.*, Apr. 2016, pp. 1430–1434.
[16] G. Litjens *et al.*, "A survey on deep learning in medical image analysis," *Med. Image Anal.*, vol. 42, pp. 60–88, Dec. 2017.
[17] A. Roche, G. Malandain, X. Pennec, and N. Ayache, "The correlation ratio as a new similarity measure for multimodal image registration," in *Proc. Int. Conf. Med. Image Comput. Comput.-Assist. Intervent.*. Berlin, Germany: Springer, 1998, pp. 1115–1124.
[18] D. Loeckx, P. Slagmolen, F. Maes, D. Vandermeulen, and P. Suetens, "Nonrigid image registration using conditional mutual information," *IEEE Trans. Med. Imag.*, vol. 29, no. 1, pp. 19–29, Jan. 2010.
[19] X. Lu, S. Zhang, H. Su, and Y. Chen, "Mutual information-based multimodal image registration using a novel joint histogram estimation," *Comput. Med. Imag. Graph.*, vol. 32, no. 3, pp. 202–209, 2008.
[20] M. Rubeaux, J.-C. Nunes, L. Albera, and M. Garreau, "Edgeworth-based approximation of Mutual Information for medical image registration," in *Proc. 2nd Int. Conf. Image Process. Theory, Tools Appl.*, Jul. 2010, pp. 195–200.
[21] S. Pradhan and D. Patra, "Enhanced mutual information based medical image registration," *IET Image Process.*, vol. 10, no. 5, pp. 418–427, May 2016.
[22] A. Andronache, M. von Siebenthal, G. Székely, and P. Cattin, "Non-rigid registration of multi-modal images using both mutual information and cross-correlation," *Med. Image Anal.*, vol. 12, no. 1, pp. 3–15, 2008.
[23] P. A. Legg, P. L. Rosin, D. Marshall, and J. E. Morgan, "Feature neighbourhood mutual information for multi-modal image registration: An application to eye fundus imaging," *Pattern Recognit.*, vol. 48, no. 6, pp. 1937–1946, 2015.
[24] D. B. Russakoff, C. Tomasi, T. Rohlfing, and C. R. Maurer, Jr., "Image similarity using mutual information of regions," in *Proc. Eur. Conf. Comput. Vis.* Berlin, Germany: Springer, 2004, pp. 596–607.
[25] J. P. W. Pluim, J. B. A. Maintz, and M. A. Viergever, "Image registration by maximization of combined mutual information and gradient information," in *Proc. Int. Conf. Med. Image Comput. Comput.-Assist. Intervent.* Berlin, Germany: Springer, 2000, pp. 452–461.
[26] H. Luan, F. Qi, Z. Xue, L. Chen, and D. Shen, "Multimodality image registration by maximization of quantitative–qualitative measure of mutual information," *Pattern Recognit.*, vol. 41, no. 1, pp. 285–298, 2008.
[27] F. Chen, D. Wu, and H. Liao, "Registration of CT and ultrasound images of the spine with neural network and orientation code mutual information," in *Proc. Int. Conf. Med. Imag. Augmented Reality*. Cham, Switzerland: Springer, 2016, pp. 292–301.
[28] C. Meng, Q. Wang, S. Guan, and Y. Xie, "Weighted local mutual information for 2D-3D registration in vascular interventions," in *Structural, Syntactic, and Statistical Pattern Recognition*. Springer, 2018, pp. 376–385.
[29] L. Juan and O. Gwun, "A comparison of sift, PCA-sift and surf," *Int. J. Image Process.*, vol. 3, no. 4, pp. 143–152, 2009.
[30] C. Studholme, D. L. G. Hill, and D. J. Hawkes, "An overlap invariant entropy measure of 3D medical image alignment," *Pattern Recognit.*, vol. 32, no. 1, pp. 71–86, 1999.
[31] M. Shadaydeh and T. Sziranyi, "An improved mutual information similarity measure for registration of multi-modal remote sensing images," *Proc. SPIE*, vol. 9643, Oct. 2015, Art. no. 96430F.
[32] D. De Nigris, L. Mercier, R. Del Maestro, D. L. Collins, and T. Arbel, "Hierarchical multimodal image registration based on adaptive local mutual information," in *Medical Image Computing and Computer-Assisted Intervention*. Berlin, Germany: Springer, 2010, pp. 643–651.